Geomechanics and Engineering, *Vol. 36, No. 3 (2024) 231-245*
https://doi.org/10.12989/gae.2024.36.3.231

Damage rate assessment of cantilever RC walls with backfill soil using coupled Lagrangian-Eulerian simulation

Javad Tahamtan*[1], Majid Gholhaki[2a], Iman Najjarbashi[1b], Abdullah Hossaini[1c] and Hamid Pirmoghan[2d]

[1]*Department of civil engineering, sanjesh parsian advanced skills Institute, Mashhad, Iran*
[2]*Department of Civil Engineering, Semnan University, Semnan, Iran*

(*Received February 26, 2022, Revised January 1, 2024, Accepted January 2, 2024*)

Abstract. In recent decades, the protection and vulnerability of civil structures under explosion loads became a critical issue in terms of security, which may cause loss of lives and structural damage. Concrete retaining walls also restrict soils and slopes from displacements; meanwhile, intensive temporary loading may cause massive damage. In the current study, the modified Johnson–Holmquist (also known as J–H2) material model is implemented for concrete materials to model damages into the ABAQUS through user-subroutines to predict the blasting-induced concrete damages and volume strains. For this purpose, a 3D finite-element model of the concrete retaining wall was conducted in coupled Eulerian-Lagrangian simulation. Subsequently, a blast load equal to 500 kg of TNT was considered in three different positions due to UFC 3-340-02. Influences of the critical parameters in smooth blastings, such as distance from a free face, position, and effective blasting time, on concrete damage rate and destroy patterns, are explored. According to the simulation results, the concrete penetration pattern at the same distance is significantly influenced by the density of the progress environment. The result reveals that the progress of waves and the intensity of damages in free-air blasting is entirely different from those that progress in a dense surrounding atmosphere such as soil. Half-damaged elements in air blasts are more than those of embedded explosions, but dense environments such as soil impose much more pressure in a limited zone and cause more destruction in retaining walls.

Keywords: CEL simulation; concrete damage; explosive blasting; Johnson-Holmquist; retaining wall

1. Introduction

Blast waves can progress from varied explosion sources such as vapor gas explosions, massive explosive charges, bursting pressure vessels, and rocket attacks. They impose significant threats to surface and underground structures (Hao *et al.* 2016a). Terrorist attacks that usually utilize explosive devices threaten lives and strategic civil structures. During explosions, a large amount of energy is released in a few milliseconds, so the blast wave propagates through the surrounding atmosphere, like air, soil, water, etc. The blast wave applies high pressure on the nearest surface of the buildings. Many researchers have investigated structures' performance under explosion hazards (Mahmoud 2019, Park *et al.* 2021), while some have tried to improve the characteristics of materials against blastings (Kim and Park 2019, Sagong *et al.* 2020). These unwanted events can be divided into inside or outside explosions. This paper has focused on both outside and inside blast loadings. External loading is typically divided into three categories due to explosion position: Free-air bursts, embedded bursts, and Surface bursts, considering the relative position of the blast source and the exploded structure (Defense 2008). this classification refers to the nature of blast wave reflection from the ground surface (Acosta 2011). whenever the blast happens near or on the ground surface, the blast load is considered a surface burst (Dadkhah and Mohebbi 2021). The experimental results can also be utilized to determine the damage rate of civil structures such as cantilever retaining walls in each explosion.

Nevertheless, experimental tests are generally challenging to secure the test site and supply exorbitant expenses. On the other hand, Surface structures such as retaining walls are not typically designed for unexpected loadings like blast waves and TNT explosions. In such a situation, retaining walls' dynamic behavior against embedded and surface blasts must be considered (Cheeseman *et al.* 2006, Koneshwaran *et al.* 2015).

Accordingly, the current paper investigates the characteristics of damages in concrete, considering the second version of the Johnson-Holmquist model using the user-subroutines in the ABAQUS software. Since retaining walls resistant against TNT loadings costs a lot, designing economical walls against massive, short-time loads exposed from embedded and surface explosions is vital for protecting these cantilever RC walls and behind materials (or even humans) during unwanted threats.

2. Lecture review

Numerical methods have been used more than ever for explosion analysis in recent years; these methods will be

∗Corresponding author, M.S.c
E-mail: javad.tahamtan@gmail.com
[a]Professor & supervisor
[b]M.S.c
[c]M.S.c
[d]Ph.D . student

ISSN: 2005-307X (Print), 2092-6219 (Online)

faster and cheaper than laboratory tests and in-situ investigations. Many authors also mentioned analytical solutions for soil-structure interaction in explosions (Li 2020, Tash and Neya 2020). Baker *et al*. (1973) stated that six parameters define soil deformation due to blast. These parameters are the depth of the embedded explosive charge, the explosive mass, the density of soil mass, the soil strength parameters, the apparent crater diameter, and the magnificent force that considers the gravitational effects (Baker *et al.* 1973). Cheeseman *et al*. (2006) have analyzed coupled Lagrangian-Eulerian to discover the explosive detonation in saturated sandy soils. In their simulation, the TNT amount, burial depth, direct distance to the structure, and cavity dimensions were studied. Ultimately, the accuracy of the simulation results was compared with laboratory test observations (Cheeseman *et al.* 2006). Tai and Tang (2006) worked on a numerical simulation of reinforced concrete slabs under standard explosion to investigate the dynamic behavior of concrete in short-time loadings. The constitutive law model of Johnson–Holmquist concrete material was used to model the high-strain states, high-pressure points in the concrete slab, and large strains. They also reveal that the Johnson–Holmquist model is able to simulate the different failure modes in concretes without any predefined defects in the element meshes.

Meanwhile, the simulated models obtain acceptable agreement between test results and the numerical simulations (Tai and Tang 2006). Ma and An (2008) used the Johnson–Holmquist material constitutive law model to simulate the models with LS-DYNA software. They manufacture the rock fractures subjected to TNT loads. Results showed that the loading rate sufficiently influences the rock fracture pattern. They state that the Johnson–Holmquist material model can effectively model tensile radial fractures and crushed compressive zones (Ma and An 2008). Luccioni *et al*. (2009) worked on the characteristics of soil deformation utilizing numerical methods and compared their results with Baker *et al*. (1991) investigations to indicate the benefits of numerical methods in predicting blasted soil changes (Luccioni *et al*. 2009).

Murthy *et al*. (2010) studied the consequence of a shock to concrete materials. For this purpose, they compared numerical analysis, experiment tests, and theoretical analysis. Finally, they stated that the limitations of present methods could cause inaccurate explanations of the failure characteristics (Murthy *et al.* 2010). De (2012) worked on surface explosions of cohesionless, unsaturated soil. This study used a fully coupled Euler–Lagrange Interaction to numerically simulate the model pressures induced by the explosions where the soil tolerates large deformations. The numerical results were close to the centrifuge model, experimental tests, and authors' field observations (De 2012). Yang *et al.* (2019) studied the damage characteristics of Reinforced concrete slabs subjected to explosions from underwater and air contact. The different responses of the Reinforced concrete slabs subjected to identical TNT mass are simulated utilizing the validated coupled method. The results indicate that the current model can represent a reliable prediction of damage characteristics for Reinforced concrete slabs while considering different blast scenarios.

The dynamic response and damage rate caused by underwater contact explosions are much larger than those of air contact explosions. However, the charge mass is the same in both situations. The concrete crush is extensively localized under the air contact blast; still, there was no observable global deformation. However, when subjected to underwater contact blasts, concrete bending and tensile failure will occur (Yang *et al.* 2019). Yang *et al*. (2019) utilized a Lagrange-Eulerian method to show a rectangular tunnel behavior while applying underwater blast loadings. They simulated the rectangular tunnel and subjected it to a range of charge weights with a horizontal distance of 2–8 m between the reference point of detonation and tunnel concrete. The damage was divided into four groups based on the deflection span ratio. Finally, they used reinforcements to improve the inner and outer tunnel lining with CFRP layers and reduce damage. The results indicate a reduction in the settlement and deflections of the tunnel lining at the top (Yang *et al.* 2019).

Oucif and Muhammad (2018) also used the second version of the Johnson-Holmquist constitutive model. They developed a model to determine the high-velocity impact on reinforced concrete panels. The outcomes emphasized that the Johnson–Holmquist damage model can predict the impact behavior of concrete slabs (Oucif and Muhammad 2018). Ambrosini and Luccioni (2020) investigated the effects of explosions on soil and structure. They state that soil density and other parameters significantly impact systems. The authors noted that the soil must be carefully selected to simulate accurately. Still, the number of damages is extensively related to the soil properties. This point emphasized the necessity of accurately defining soil parameters when observing the behavior of civil structures in contact with soils subjected to blast loadings. For this goal, structures must be modeled explicitly (Ambrosini and Luccioni 2020).

3. Blast

Standards for the stability of numerous civil structures, such as retaining walls against buried and surface blasts, had been discussed (Station 1986). An extensive energy release accompanies an explosion in only a few milliseconds; this process causes a shock wave to propagate in the environment and fill the surrounding air or soil with a compressive wavefront. Meanwhile, A high-level pressure will be applied to any material in the surrounding environment. The shock wave moves forward radially from the detonation point; hence, increasing radius will reduce velocity. The wavefront progresses across a large volume, and the explosion pressure (Pso) value decreases simultaneously (De 2012). Generally, vibration waves' properties include amplitude, period, and frequency affected by the soil, ground geometry, soil topography, dispersion, and absorption. Research of numerous regions reveals that sites hardly affected by explosions are typically restricted to a small area (Uyar and Aksoy 2019).

A surface explosion causes large deformations and increases the strains and stresses in the surrounding soil.

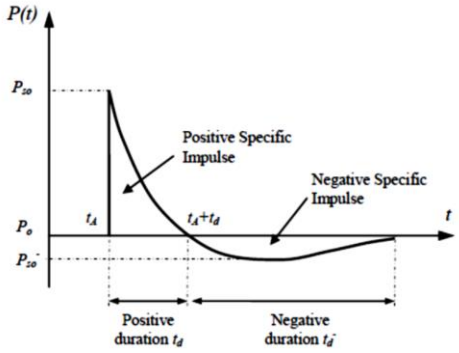

Fig. 1 Incident pressure's time history

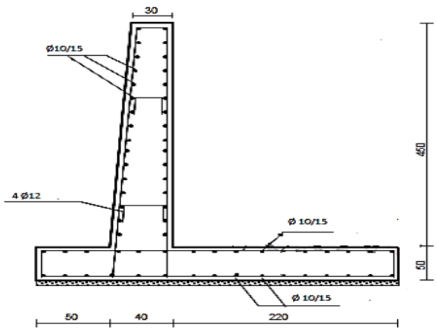

Fig. 2 Geometry dimensions and reinforcements (centimeter)

These changes are consequences of the interaction between the surrounding soil and induced compressive waves. These deformations highly depend on the hydraulic conditions of the explosion and the soil characteristics (Osinov *et al*. 2019). The time history of pressure during a blast has been studied by different researchers (Brode 1955, Hao *et al*. 2016b). A usual shape of blast pressure is demonstrated in Fig. 1. Fig. 1. shows that the blast pressure can start with an initial positive phase and then turn into its negative phase. The following Equation represents the blast pressure during time (Bulson 1997).

Here, p(t) is the pressure caused by the blast in time (t). this pressure is measured from t_A, which is the explosion arrival time. P_0 is equal to surrounding air pressure, which is 101 kPa in most cases. Also, P_{so} is the peak incident pressure in the trace, and t_d is the positive phase time; the decay coefficient (b) is vital in extending the explosion in the negative duration. When b<1, the extension of the negative duration is significant; in the cases where b≥1, the extension of the negative duration can be neglected (Baker *et al.* 1973). The previous authors have demonstrated various empirical equations and graphs to explain the peak incident pressure (Henrych and Major 1979, Kinney and Graham 2013, Wu and Hao 2005). These authors indicated that the peak incident pressure is affected by the scaled distance parameter and can be expressed as follows (Bulson 1997)

$$z = \frac{R}{W^{\frac{1}{3}}} \quad (1)$$

Here, R is the direct distance from the reference point (m), and W is equal to the equivalent weight of TNT (kg).

The following factors can impact the value of the explosion pressure (Station 1986):

- Distance to the structure and the quantity of charge
- Dynamic behavior of soil
- Depth of embedded explosion charge

4. Methodology

The reinforced concrete cantilever wall and beside soil was modeled in ABAQUS CAE for the Finite Element simulation. This program was used to assign material properties, apply interaction and boundary conditions, and mesh the Eulerian and Lagrangian parts. The element used for modeling soil, internal steel reinforcement, air, and retaining wall is an 8-node linear brick with reduced integration and hourglass control, also known as C3D8R in the Lagrangian model. Also, the EC3D8R element is used for the Eulerian part. A finite element model is progressed to represent the damage rate of concrete cantilever retaining walls in various positions using 500 kg of TNT.

For this simulation, a mesh convergence investigation was considered to determine the impact of the aspect ratio of the C3D8R elements on the ultimate results of using an optimal FE mesh that obtains a relatively accurate solution with the lowest computational costs. Elements with an aspect ratio of 1 (in most cases) and not higher than 1.5 in the whole model resulted from optimal meshing for the numerical simulations. To increase simulation accuracy, the meshing was densified nine times more in the retaining wall, TNT, and reinforcement areas.

For the solid model (Lagrange Model), the structure's mesh is set to 250 mm, but for the air model (Euler Model), the mesh is set to 200 mm.

As far as the TNT load exploding in the middle of the length in all positions, the regions' width was set to 12 m, which is suitable as no boundary effect was observed in the results. The backfield soil and front air length equals 20 m, where the boundary is far enough from the wall face. Furthermore, the height of the wall is considered to be 5 meters. Other dimensions of the retaining wall are shown in Fig. 2.

The dimensions and properties of the cantilever concrete wall and internal reinforcements are given here. These properties are sufficient for tolerating dead, live, and earthquake loads according to Iranian earthquake Standard no. 2800. The perfect condition for modeling an infinite boundary is to simulate a more significant size model; therefore, the desired structure could not be affected by the reflection of stress wave (Wang *et al*. 2019), but this approach is time-consuming and not practical in general. Regarding Fig. 3, transmit boundary conditions in the Eulerian mesh on the outer surface of the model were considered to prevent the shock wave's reflection from the explosion at the boundary of soil mass. Hence, the flow-out condition was utilized in the border of soil, cantilever wall, and air elements to simulate better the volumetric expansion effect. The bottom was considered bedrock without displacement or reaction forces being allowed.

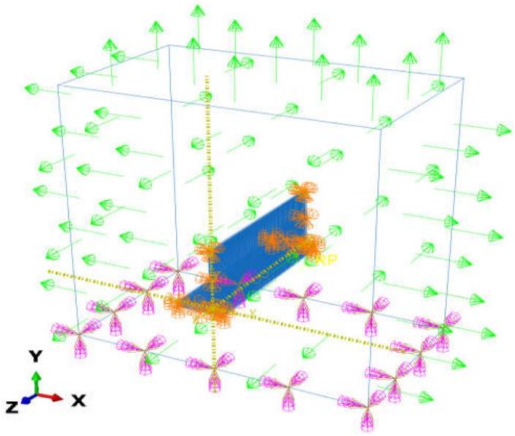

Fig. 3 Transmit and bottom boundary condition

5. Constitutive model

A proper constitutive model selection for each material, such as air, soil, steel, and concrete, plays a vital role in the precise numerical modeling of explosions (Hejazi *et al*. 2008).

5.1 Soil constitutive model

The soil mass in the current paper was modeled as an isotropic continuum with yielding that is described by the Mohr-Coulomb yield criterion as

$$\tau = c + \sigma_n \tan \varphi \quad (2)$$

In Eq. (2), c is the value of cohesion in the soil, σ_n is the normal vertical stress, φ is the internal friction angle, and τ is the shear stress. Also, a small cohesion value of 1 KPa has been assumed for the sandy soil. Internal friction angles of 35° and a dilation angle of 5° were considered (Rahgooy *et al*. 2022).

The concrete foundation had a modulus of elasticity (Ec) of 2.1 GPa and a Poisson's ratio (μ_c) of 0.2. The soil had a modulus of elasticity (Es) of 10 MPa and a Poisson's ratio (μs) of 0.3. The specific weight of concrete (γc) in the foundation and soil (γ) were 2400 and 1810 kg/m3, respectively (Rahgooy *et al*. 2022).

The Lagrange processor is generally ideal for the behavioral analysis of solids materials; the Lagrange processor is specified for the cantilever retaining wall. In contrast, the Euler processor is typically perfect for the behavioral analysis of fluids; therefore, in this paper, the Euler processor is used for the air, soil, and TNT materials. The current approach also had been used in (Jeon *et al.* 2015).

5.2 Steel constitutive model

Using the elastoplastic law, this paper modulates horizontal bars and stirrups in the retaining wall. In this constitutive law model, whenever any element reaches the maximum plastic strain during the blast loadings, the element is regarded as failed. The S420 Steel was considered for reinforcement with a density of 7800 kg/m^3, elasticity (Ec) of 200 Gpa, Poisson's ratio (μs) of 0.3, Tensile Strength of steel used in cantilever wall is 420 Mpa and Compressive Strength of 420 Mpa.

5.3 Air constitutive model

Atmospheric characteristics are not constant in different situations and can vary extensively. The model should use precise values that perfectly reflect the blast site conditions. Abaqus has some ways the simulation can represent air characteristics in different states.

In a surface burst, shock wave stress is moved forward and attenuated by an increased radius. So, a suitable constitutive model for air material should be utilized to model the charge explosion. The air does not consist of yield strength and acts in a fluid-like manner (Wang *et al*. 2019). A typical model in Abaqus is the one with an ideal gas state equation. This Equation considered the reference mass density of 1.2 kg/cm3 and specific heat of 717.1. An equation of state governs the correlation between pressure and volume, and the gas constant is equal to 287 while ambient pressure is 101325 pascal and dynamic viscosity is equal to 8.25E-05 m/s.

6. Interactions

Considering good contact between stirrup and longitudinal rebars and covered concrete is vital in the blast simulation because the stress flow among different parts affects the dynamic behavior of materials (Abedini *et al*. 2019). This paper considers the internal steel reinforcement an "embedded element" in the concrete retaining wall. Here, the wall acts as a host. So, embedded nodes will have an identical translational degree with the surrounding host elements. This strategy reasonably assumes that no sliding between internal steel and concrete occurs under compression (Zhao *et al.* 2012). The same interactions were also defined between the heel and toe concrete of the retaining wall and the steel angles. The latter assumption allows the definition of perfect contact between steel angles and concrete (avoiding potential convergence problems due to other types of contact modelling). Also, a general contact (explicit) interaction was used to define the contact properties between the steel rebars and closed stirrups. When the TNT arrived the retaining wall, there will be no friction in their contact.

7. Verification

This paper benefits from commercial numerical software, so it generally does not utilize a new equation. However, the authors define the subjected innovative models (second version of the Johnson-Holmquist model) for the analysis and import the required data as they need. Therefore, verifying whether the analysis results simulate the actual behavior would be necessary.

Tuğrul and Sevim (2017) performed a numerical study

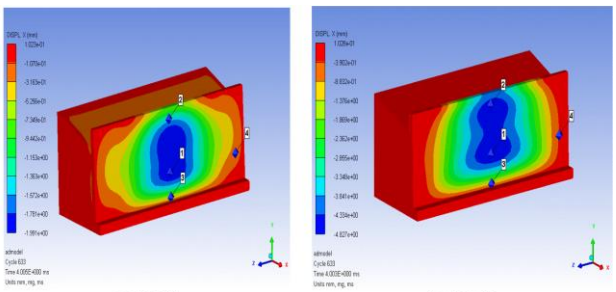

(a) Model-1 (b) Model-2

Fig. 4 Displacement contour diagrams of the models at X direction (mm)

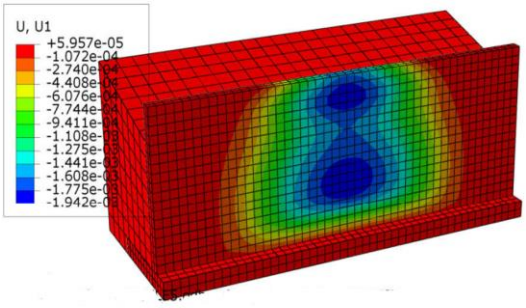

Fig. 5 Displacement counter with the same direction of simulating model-1 in Abaqus (m)

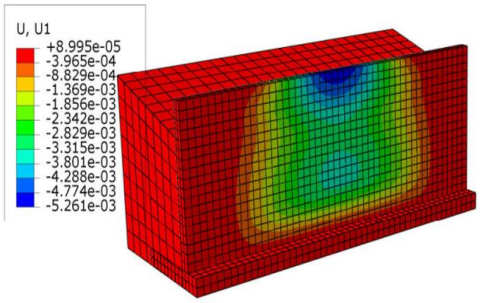

Fig. 6 Displacement counter with the same direction of simulating model-2 in Abaqus (m)

to evaluate the displacement of the RC retaining wall under TNT explosives (Tuğrul and Sevim 2017). They performed two explicit models in ANSYS AUTODYN software. In model-1 (Fig. 4(a)), the horizontal distance between the explosive material and the structure equals 5.5 m. In model-2 (Fig. 4(b)), the horizontal distance equals 4 m. in Both positions; the explosive load is meshed and simulated with the air (Euler) model. The density of the TNT is 1600 kg/m3, and the mass of the TNT is equal to 410 kilograms.

The detonation of the explosives for both models is at the center of the TNT volume. The same model has been simulated in Abaqus software utilizing the concept model to verify the result. Fig. 4 shows the result in Ansys and Figs. 5-6 Show the verified model in Abaqus. The compared result is shown in Fig. 7. As shown in Fig. 7, the results in the two programs are almost identical, so the current software can also consider a new constitutive model for retaining walls with the same geometry.

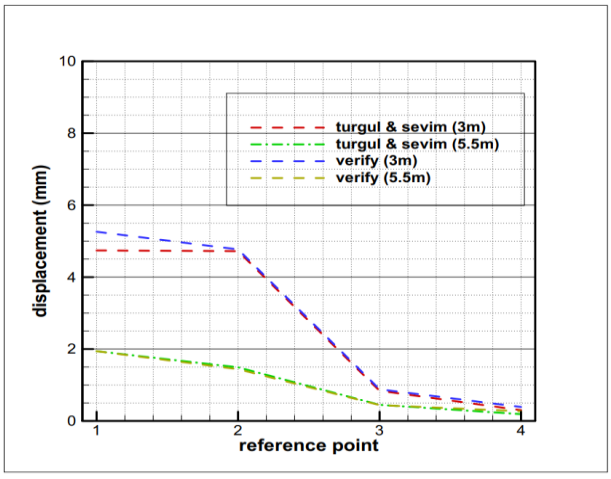

Fig. 7 Comparing horizontal displacement in gauge points (mm)

8. Computational algorithm

A computational algorithm must be considered before performing a model. It will enable the explosion waves to pass through the target grids in the computation process. The three possible computational approaches are (Schwer and Day 1991):

(a) Rezoning: after solving a certain number of cycles, some grids will be destroyed, and the rezoning algorithm will map them into a more regular grid, e.g., a new grid will form after the target zones in front of a mass charge become hardly compressed. This technique is typically very time-consuming and is not available in all software.

(b) ALE: This algorithm benefits from the advantages of the Eulerian and Lagrangian techniques. In this scheme, defined nodes in the computational grid are placed in a restricted position in model space, although they can move with the material or progress in the prescribed manner.

(c) Eroding elements: The eroding algorithm rectifies the problems related to highly distorted elements in blast simulations by deleting parts that reach the removal criteria of grids. The requirements are generally heuristic and defined with the maximum allowable values of the element's deformation or stress measures; this could be expressed through an effective plastic strain or principal stress of materials.

This paper Benefited from the coupled Euler-Lagrangian method and eroding elements method to find out the intensity of the explosion beside and in front of a cantilever retaining wall.

9. Characteristics of explosives

There are many ways to introduce explosives load in ABAQUS, but the most prevalent one in simulations is the JWL[1] state equation. Inherently, JWL is a physical model;

[1] Jones-Wilkins-Lee

Table 1 JWL EOS properties for explosive load

type	ρ_o (kg/m3)	R_1	R_2	A (pa)	B (pa)	w	e_0 (j/m3)	P_{cj} (pa)	VOD (m/s)
TNT	1630	2.63	2.62	$3.738e^{11}$	$3.747e^{6}$	0.35	6e9	$2.1e^{10}$	6930

*ρ_o = explosives' density,
e_o = the Initial Chapman-Jouguet energy,
P_{CJ} = pressure of Chapman-Jouguet,
VOD = Chapman-Jouguet detonation velocity

therefore, this model can simulate chemical explosives too. In this manner, JWL uses thermodynamics law (Manual 2020). In this paper, the explosive load equals 0.5 tons of TNT with a 1630 kg/m3 density. Table 1 shows the coefficients of TNT used in the current paper for the JWL equation (Manual, 2020).

The Jones-Wilkins-Lee Equation (JWL) has progressed considering the relation between the pressure of explosive material and its volume expansion. It can be observed with the help of the cylinder expansion test. The JWL equation is shown as Eq. (3)

$$p = A(1-\frac{\omega\eta}{R_1})e^{-\frac{R_1}{\eta}} + B(1-\frac{\omega\eta}{R_2})e^{-\frac{R_2}{\eta}} + \omega\eta\rho_0 E \quad (3)$$

In the Equation, η is the detonation product density ratio divided by the explosive's initial density. A, B, R_1, R_2, and ω are fitting coefficients, as mentioned in Table 1. Also, the explosives for each model are detonated at the center of the TNT.

10. Johnson-Holmquist-2

Concrete is one of the most complex materials due to its inconstant behavior in various loading situations (Akram and Yesilyurt 2023). Many constitutive law models have progressed in recent years to comprehensively describe the dynamic behavior of concrete under Short-term loads such as explosive ones. In the current paper, the modified Johnson Holmquist constitutive law model, also called JH-2, is utilized to observe the brittle behavior of concrete in cantilever RC walls facing the explosive load in different positions. JH-2 is the innovative and modified prescription of the old Johnson–Holmquist model (Johnson and Holmquist 1992). The new model is generally suitable for simulating the behavior of brittle materials, such as concrete, under impact loads. This constitutive model considers the pressure-strength dependency of materials, dilatation, and strain-rate influences. In the old model named JH-1, the yielding strength is reduced whenever a defined critical value of the damage is reached. Instead, the yielding strength reduces with the rate of damage accumulation in the new model. The strength in the JH-2 model is defined as equivalent stress, which is

$$\sigma^* = \sigma_i^* - D(\sigma_i^* - \sigma_f^*) \quad (4)$$

where

σ_i^* = the normalized intact equivalent stress.

D = damage variable.

σ_f^* = the normalized fractured equivalent stress.

The material's undamaged and completely damaged values are defined with D=0 to D=1.

Instead of the above Equation, the strength is considered to normalize Eq. (4) to the Hugoniot elastic limit's equivalent stress. Hugoniot elastic limit is defined as a shock wave in one dimension that passes the elastic limit

$$\sigma_{HEL} = \frac{3}{2}(HEL - P_{HEL}) \quad (5)$$

In Eq. (5), the pressure at the HEL is called P_{HEL}. After normalization, Eq. (4) would be

$$\sigma^* = \frac{\sigma}{\sigma_{HEL}} \quad (6)$$

According to the JH-2 constitutive law model, the Equation of the strength can be represented with strain rate and pressure rate in undamaged and completely damaged brittle material as follows

$$\begin{aligned} \sigma_i^* &= A(P^* + T^*)^N (1 + C\ln\varepsilon^*) \le \sigma_i^{\max} \\ \sigma_f^* &= B(P^*)^M (1 + C\ln\varepsilon^*) \le \sigma_f^{\max} \end{aligned} \quad (7)$$

A, B, C, N, and S_{max} are the material constants.
A = material's normalized cohesive strength
B = coefficient of normalized pressure hardening
C = coefficient of strain rate
N = pressure hardening exponent
S_{max} = normalized maximum strength.

Therefore, the normalized pressure is

$$P^* = \frac{P}{P_{HEL}} \quad (8)$$

P = the current hydrostatic pressure.

Hence, the normalization of maximum tensile hydrostatic pressure is considered as follows

$$T^* = \frac{T}{T_{HEL}} \quad (9)$$

T= is the maximum value of tensile pressure supported by the brittle material. In this condition, the strain rate is equal to

$$\varepsilon^{\dot{P}l} = \frac{\bar{\dot{\varepsilon}}^{Pl}}{\dot{\varepsilon}_0} \quad (10)$$

$\bar{\dot{\varepsilon}}^{pl}$ = the equivalent plastic strain rate.

The modified Jonson Holmquist constitutive law model utilized the same damage accumulation as the Johnson-Cook constitutive law model. The Johnson-Cook generally assumes that the damage rises whenever the plastic strain is increased, which is

$$\begin{aligned} D &= \sum \frac{\Delta\bar{\varepsilon}^{pl}}{\bar{\varepsilon}^{pl}(P)} \\ \bar{\varepsilon}^{pl} &= D_1(P^* + T^*)^{D_2}; \bar{\varepsilon}_{f_{\min}}{}^{pl} \le \bar{\varepsilon}^{pl} \le \bar{\varepsilon}_{f_{\max}}{}^{pl} \end{aligned} \quad (11)$$

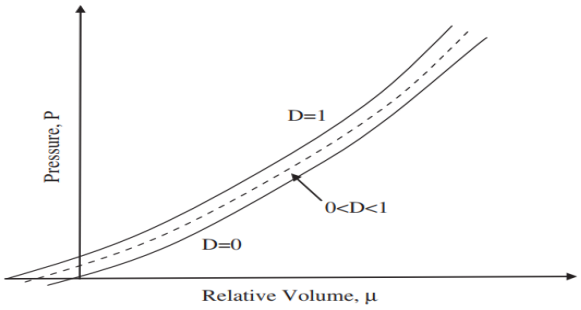

Fig. 8 Relation of Pressure and volumetric strain of the JH-2

$\Delta\bar{\varepsilon}^{pl}$ = the increment of equivalent plastic strain

$\bar{\varepsilon}_f^{pl}$ = the equivalent of plastic strain at failure.

D_1 and D_2 = material constants.

$\bar{\varepsilon}_{f_{min}}^{pl}$ & $\bar{\varepsilon}_{f_{max}}^{pl}$ = maximum and minimum of fracture strains.

The pressure-volume relationship in JH-2 for brittle material is

$$\begin{cases} K_1\mu^2 + K_1\mu^2 + K_1\mu^3; \ \mu \geq 0 \ (compression) \\ K_1\mu; \ \mu \leq 0 \ (tension) \end{cases} \quad (12)$$

K_1, K_2, and K_3 =constants

$\mu = \frac{\rho}{\rho_0} - 1,$

ρ = the current densities

ρ_0 =reference densities.

In JH-2, When the material reaches the failure criterion in some elements, an additional pressure increment ΔP is added, which is

$$P = K_1\mu^2 + K_1\mu^2 + K_1\mu^3 + \Delta P \quad (13)$$

The determination of the pressure increment is through the energy considered, meaning that whenever the material is partly damaged, the deviatoric elastic energy DU is immediately reduced owing to the strength reduction. Fig. 8 reveals the current model's relation between the pressure and volumetric strain. JH-2 has the same parameters as the old version, namely D1, D2, and EF_{MIN}. These parameters are obtained from cyclic uniaxial compression tests. It should be noted that EF_{MIN} is the minimum plastic strain before the initialization of fracture. Still, most authors initially used the D1=0.04 and D2=1 (Kucewicz *et al.* 2021). The JH-2 method is considered a homogenization of the simulated material. Therefore, it assumes no imperfections or discontinuities (Kucewicz *et al.* 2020). The reduction of elastic energy is then converted to potential energy. This trace will happen through a raise in the pressure increment, which is equal to

$$P = K_1\mu^2 + K_1\mu^2 + K_1\mu^3 + \Delta P \quad (14)$$

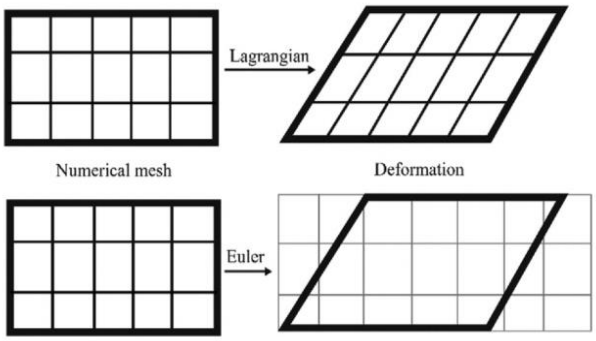

Fig. 9 Lagrange and Euler mesh behavior Schematically (Rashiddel *et al.* 2020)

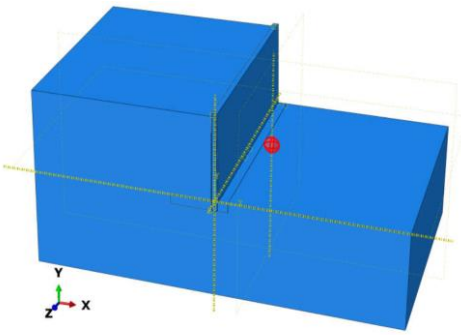

(a) explosion in front of a wall (scenario1)

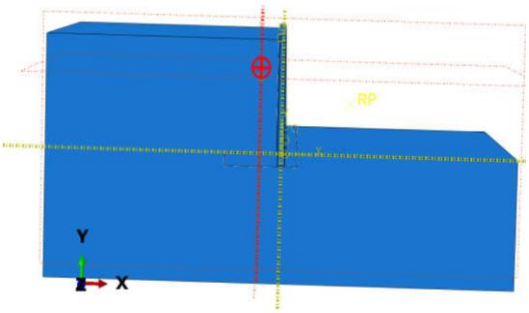

(b) explosion in the middle of soil (scenario2)

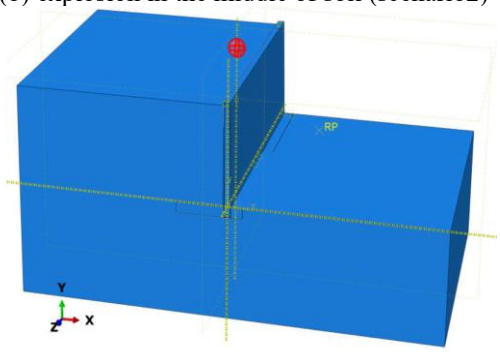

(c) explosion above the soil (scenario3)

Fig. 10 Relatively position of TNT, soil, and the cantilever wall

β = the fraction of the elastic energy increase converted into potential energy $(0 \leq \beta \leq 1)$. Table 2 shows the parameters used in the JH-2 model in the current paper.

Table 2 JH-2 properties for concrete

ρ_0	A	N	B	M	C	e_0
2400	0.79	0	1.6	0.61	0.007	1.0
HEL	P HEL	SigI Max	sigFMax	beta	D1	D2
80E6	48E6	8.6E9	1.1E9	1.0	0.04	1.0E
efMax	efMin	T	K1	K2	K3	FS
1.0	0.001	0.00354E9	85E9	-171E9	208E9	0.2

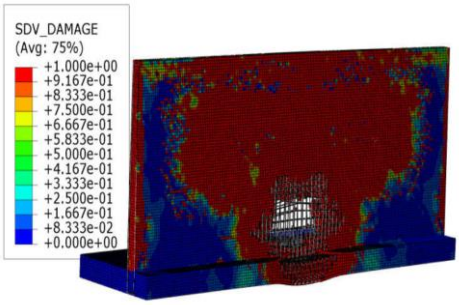

(a) effective explosion time of 0.003

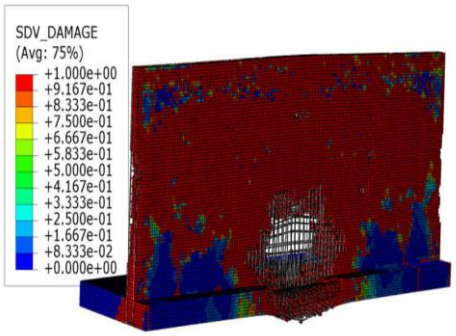

(b) effective explosion time of 0.007

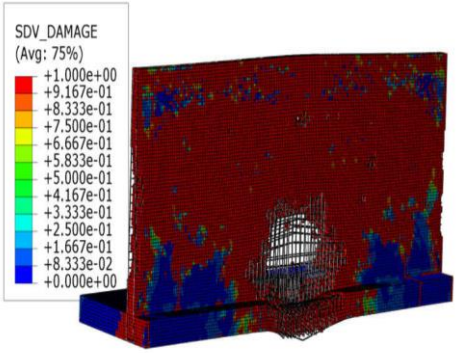

(c) effective explosion time of 0.007

Fig. 11 Damage ratio in the concrete of retaining wall in scenario 1 using the JH-2 model

11. Fully-coupled Euler–Lagrange formulation

The most familiar solvers in explosion simulation are Euler, Lagrange, conwep, Arbitrary Lagrange Euler, and Smooth Particle Hydrodynamic. Meanwhile, an innovative, fully coupled interaction exists between the Lagrangian and Eulerian methods (De 2012, Khodaparast *et al.* 2023). The CELM showed an accurate structure based on particle distribution (Jin *et al.* 2023). So, proper constitutive law models must be accurately selected to simulate the behavior of different materials against blast waves. The current paper adopts a coupled Eulerian-Lagrangian formulation to simulate blast loads precisely in fluid-solid interaction. The full coupling of Lagrangian and Eulerian lets the model deform as much as needed, while solids generate fluid-solid boundaries (Choi *et al.* 2006).

Here, the solid phase is a cantilever retaining wall, and the fluid phase includes surrounding air, blast waves, and exploded soil. According to Fig. 9, the numerical mesh remains intact in the Euler method. At the same time, the materials can flow from one element to other elements freely. The deformed shape will be simulated by mesh distortion. This method is proper for fluid-phase materials, like surrounding air or TNT mass (De 2012).

12. Results

This section evaluates three scenarios, as shown in Fig. 10. In the first scenario, the explosion occurs in front of the retaining wall. In scenario two, the explosion load had been embedded in the soil with a burial depth of 2 meters. Finally, in scenario three, the explosion load is considered on the top of the backfilled soil.

12.1 Scenario-1

In this scenario, the direct distance from the bottom-middle of the wall is 1 meter to 5 meters, and other parameters are constant (Fig. 10(a)). The damage rate based on the johnson-Holmquist-2 approach (user-subroutines) is shown in Fig. 11 for the most critical positions of 1 meter in scenario one, with effective explosion times of 0.003, 0.007, and 0.01 seconds, respectively. As shown in Fig. 11, increased explosion time will increase the concrete damage rate. Meanwhile, the most damages are experienced in the initial steps; more than 80% of concrete damages came in just 0.005 seconds.

Meanwhile, a deflection in rebars, especially at the toe of the cantilever wall, is noticeable. Also, the result shows that the mean of von Mises stresses in rebars will decrease with increased distance between the RC wall and TNT. As shown in Fig. 12, The mean stress in all longitudinal rebars and closed stirrups is almost 265 MPA in the first 0.002 seconds, where the distance between the RC wall and TNT is 1 meter. After that, a slight drop will occur, resulting from a negative specific impulse and a smooth increase in stress. This point reveals that the TNT blast effective time may not be the most critical parameter in short distances. As shown in Fig. 12, the immediate peak will vanish by increasing the distance, and the peak stress will happen within a bit of delay. The latest peak belongs to a 5-meter distance where it takes 0.006 seconds to reach the maximum mean of 100 MPA in steel. Also, it could be concluded that by increasing the distance to more than 2 meters, the maximum mean stress will dramatically fall. Although still in all cases, the highest stress is observed in middle steels where the concrete is destroyed entirely, and no cover remains for steels. (Sagong *et al.* 2020) The same trend was reported for shear stresses in the tunnel lining material.

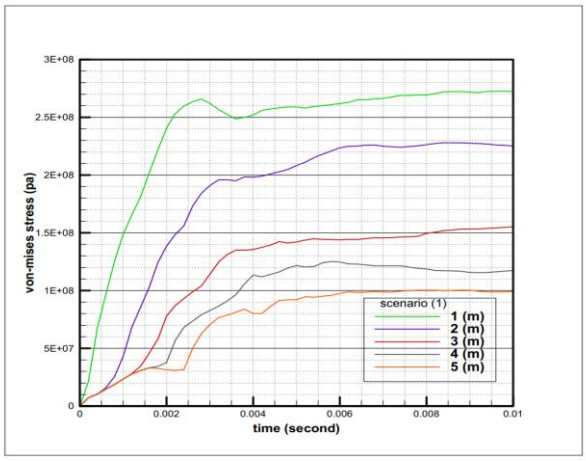

Fig. 12 Mean von Mises stress of steels in scenario 1

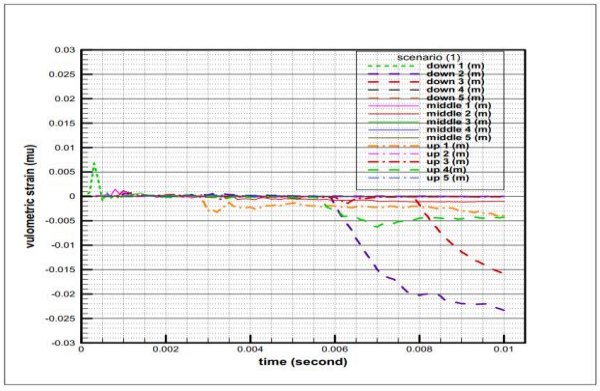

Fig. 13 Volumetric strain at gauge points in scenario 1

Also, user-subroutines considering volumetric strains in concrete parts were available. For this purpose, three gauge points were considered in the bottom, middle, and top of the retaining wall, just in front of the explosion load. As shown in Fig. 13 for scenario 1, the bottom point, nearest to the explosion loads, reveals the more volumetric strains up to 0.025. this point is where the RC wall tolerated the most damage in concrete. Also, firstly, the volumetric strains rise with an increase in the distance, but after 2 meters, they decrease in all cases.

12.2 Scenario-2

In this scenario, the blast wave progressed from the buried charge in the soil. This paper simulated the blast consisting of 500 kg of TNT located 2.5 m beneath the surface within a 1-to-5-meter horizontal distance from the middle of the retaining wall. Flow-out boundary conditions are considered to avoid the boundary wave's reflection. As shown in Fig. 14, the cantilever RC wall has the most damage in scenario two, where the explosion load is embedded in the soil environment. In this scenario, an extensive area faces complete damage, so the element has been deleted due to the entire damage in concrete material. The RC wall also tolerates a huge deflection in middle rebars.

There are three reasons for this event; first, the higher density of soil than air increases the pressure load on the

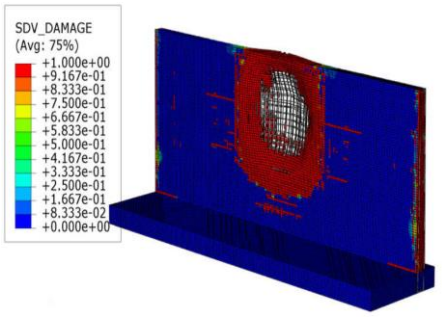

(a) effective explosion time of 0.003

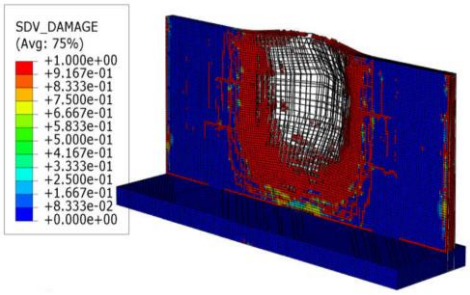

(b) effective explosion time of 0.007

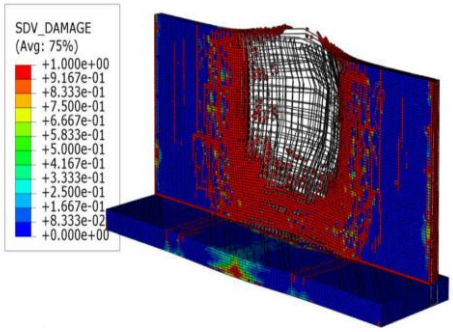

(c) effective explosion time of 0.01

Fig. 14 Damage ratio in the concrete of retaining wall in scenario 2 using the JH-2 model

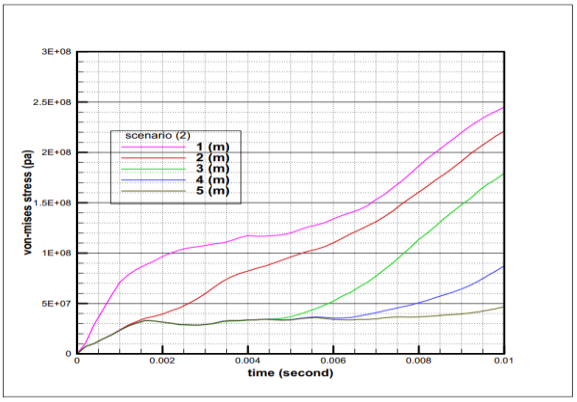

Fig. 15 Mean von Mises stress of steels in scenario 1

retaining wall significantly. Second, in scenarios one and three, a fast upward movement of blast waves causes less pressure on the wall, while in scenario two, the contact with a higher number of waves. Third, in scenario one, a backfill helps the wall resist deformation, while in scenarios two and three, the retaining wall can move back quickly. As a result, a higher

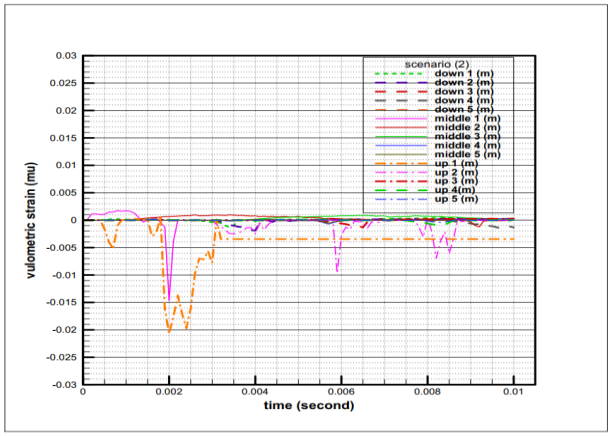

Fig. 16 Volumetric strain occurred at gauge points in scenario 2

moment will apply to the foot of the wall (especially in scenario three). (Liu *et al*. 2019) indicated that the detonation of a concentrated blasting load has a significant effect on the damages of materials in the near zone of the explosive load coordinates and a more negligible effect at a far distance, which is observed In Fig. 14. In scenario two, geological structure and soil density are more pronounced. As reported by (Shadabfar *et al*. 2020), The size of the blast load-induced damages was extensively reduced by raising the distance between the embedded blast charge and the wall, which happened in three scenarios and was more evident in scenario two.

Analyzing Fig. 15 shows that the delay in von Mises's peak point is evident compared to scenario one. The reason is that the wave will progress at a lower speed in a dense medium such as soil; therefore, the impact will occur later than in scenario one. Also, the negative specific impulse is not evident in this scenario; instead, the drift in soil mass will cause a massive force beside the RC wall. Here, in scenario two, the wall faces higher steel pressure. Fig. 15 reveals that the maximum mean stress in steels is almost 250 MPA, related to a 1-meter distance. Here, a dramatic drop in von Mises stresses occurs when the distance exceeds 3 meters. Also, the stresses will rise significantly after 0.06 seconds, and there is no peak point during analysis. Other investigations also state that soil drift greatly influences blast loads' impact on targets located; in the study of Swinton and Bergeron (2004), a 40 cm in radius and 50 cm deep steel container was considered in the medium-dry sand. Five tests with different TNT weights were modeled, and the result shows that it took between 30 milliseconds to 50 milliseconds before initializing any movement in soil (Swinton and Bergeron 2004). For scenario two, the volumetric strain in the gauge points is shown in Fig.16. Comparing Fig. 16 with Figs. 14 and 18 indicates that scenario two has a lower volumetric strain in gauge points. Here, the most expansions will occur in the middle and top of the wall, while in scenario one, the toe of the wall has the most expansions. The peak of volumetric strains happens in the middle and top of the RC wall when the TNT explodes at a 1-meter distance. The volumetric strain will become more similar by raising the distance in different positions.

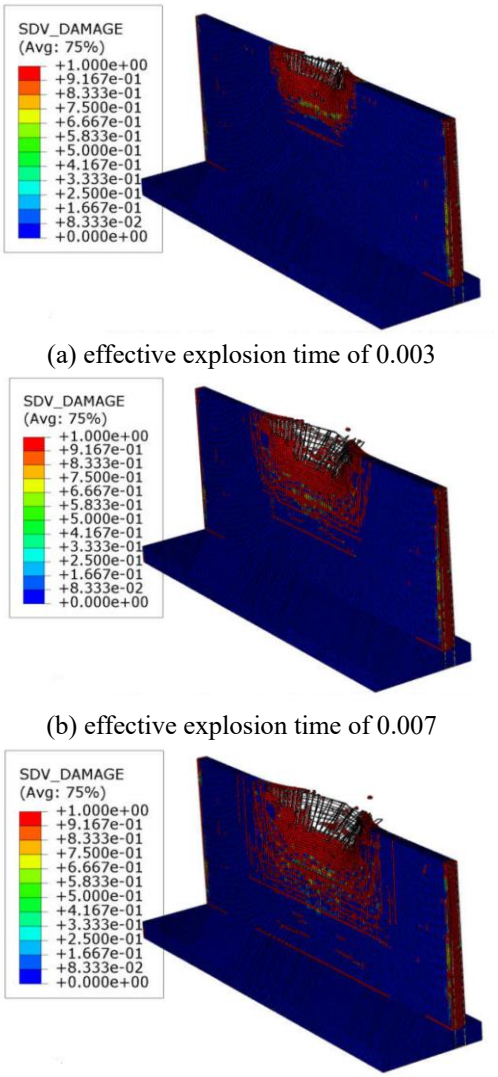

(a) effective explosion time of 0.003

(b) effective explosion time of 0.007

(c) effective explosion time of 0.01

Fig. 17 Damage ratio in the concrete of retaining wall in scenario 3 using the JH-2 model

12.3 Scenario-3

As shown in Fig. 10(c), The TNT exploded above the soil in scenario three. In this case, the drift of soil mass and the bending moment of the RC wall are the most critical concerns. Still, a significant portion of released energy will progress in the air (Fig. 17). Therefore, this scenario faced much less concrete material damage and less stress in steel. Fig. 18 Shows the mean von Mises stress in steels. Here, the wall meets the maximum stress at the end of the blasting time while the distance is less than 3 meters; meanwhile, by an increase in space between the TNT and wall, the peak will occur in the first 0.004 seconds; after that, the stresses will decrease. As shown in Fig. 19, the volumetric strains increase by increasing the distance in scenario three. Hence, the most strain will occur at the top of the wall with a magnitude of -0.045. Although the stresses and damages in scenario three are less than the two other ones, having a higher volumetric strain will be an important hazard for the RC walls.

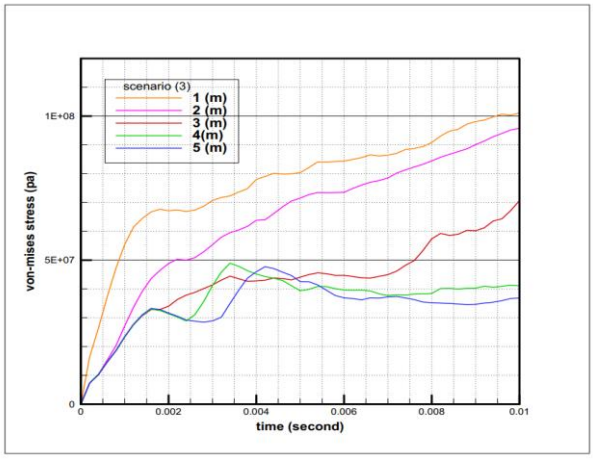

Fig. 18 Mean von Mises stress of steels in scenario 1

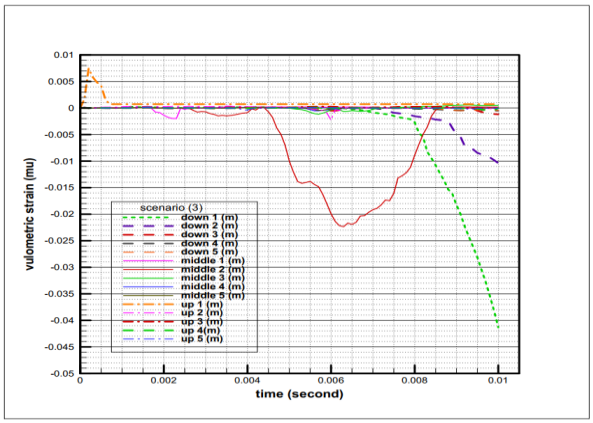

Fig. 19 Volumetric strain occurred at gauge points in scenario 3

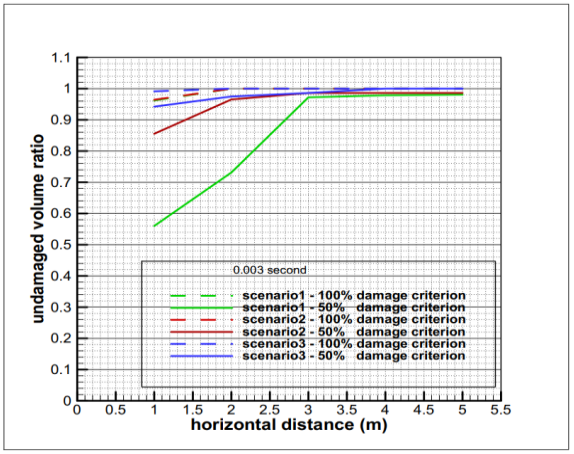

Fig. 20 Damage criteria for 0.003 seconds

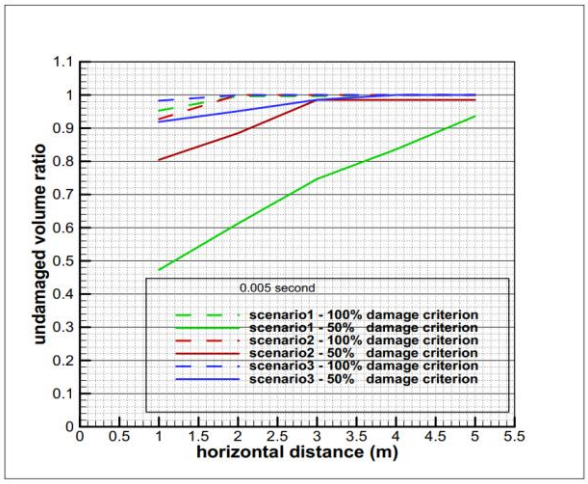

Fig. 21 Damage criteria for 0.005 seconds

12.4 concrete damage rate in different scenarios

When the blast waves progress, the middle of the wall will face significant pressure. Then, the internal strain in the concrete is disturbed and propagates to the double side of the retaining wall in compressional waves. In the following, the waves reflect, serving as tensile waves. When the tensile stress generated by the reflected wave is more significant than the sum of tensile strength and the compressional stress, the concrete will start to spall and disrupt. The increased shearing and bending stresses will cause the disruption of the material within the coarse aggregate and lead to a higher damage ratio of the concrete (Sun and Liu 2022).

The result indicates that the maximum von Mises stresses and the highest amount of volumetric strain are those that happened in the middle of the wall, where the distance between TNT and the surface of the wall is minimal. Due to the unidentical radical proration of blast waves in 3 scenarios, the concrete damage rate must differ in various positions. However, the elements with complete damage are in the middle of the wall.

In analyses, the element with D=1 in 8 edges of the element considered complete damage and deleted immediately; these elements are eliminated and considered in 100% criterion and reduce the volume of the remaining wall. On the other hand, in some elements, especially those located between the entirely damaged element and boundaries of the wall, some elements have not experienced D=1 in 8 edges but tolerated at least D=0.5 in them; these elements are not eliminated and considered as %50 damage criterion. Figs. 20 to 23 show damage criteria for 0.003 seconds, 0.005 seconds, 0.007 seconds, and 0.01 seconds, respectively.

As shown in Fig. 20, The most damage in all positions is related to the 1-meter distance where the TNT is in the nearest place. Still, scenario one has the most %50 damaged elements where almost 0.44 of the total concrete volume has been experienced D =0.5 in all edges. After that, in scenario two, nearly 0.15 of the entire concrete volume has been experienced D=0.5. The result shows no apparent difference between damage rates in various scenarios by increasing distance to more than three meters. By increasing the distance to more than 3 meters, we do not face any element with D=1 due to low blast effective time and almost a far distance; there are just a few elements with D=0.5 or less Limited to %5. Fig. 21 Shows the result of two criteria for an effective blasting time of 0.005 seconds.

As shown in Fig. 21, By increasing the effective time, for scenario one, there will be at least %52 half-damaged elements

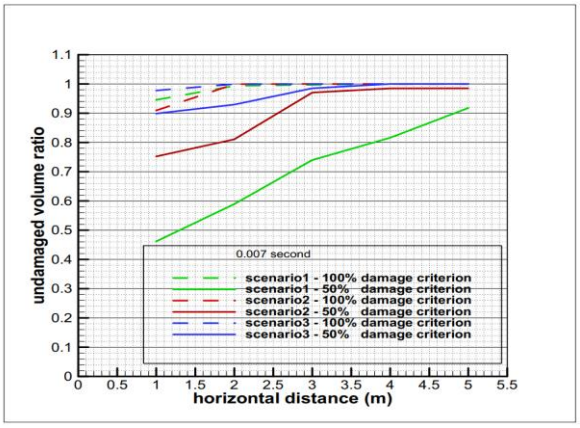

Fig. 22 Damage criteria for 0.007 seconds

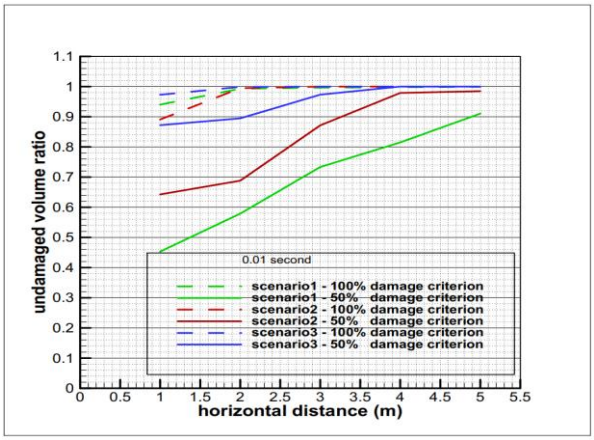

Fig. 23 Damage criteria for 0.01 seconds

in a 1-meter distance and %6 of the half-damaged elements in a 5-meter distance, which is significantly more than the results of 0.003 seconds. This fact reveals that effective blast time has a massive impact on retaining wall damage. The element with D=1 has also increased in all scenarios in 0.007 seconds. However, after increasing the distance to more than 3 meters, almost identical results were observed where the element with all damages tipped to zero. Fig. 22 Shows the result for 0.007 seconds of blasting time. The important conclusion from Fig. 22 is that, although in all cases, the half-damage in scenario 1 is more than in other scenarios, the volume with complete damage in scenario 2 passes scenario 1, which means that more concentrated pressure will apply to the middle of the wall in scenario 2 and those the wall tolerate more deformations in the middle too; the result will be due to the drift which occurs in soil volume, as previously investigated in (Swinton and Bergeron 2004).

As shown in Fig. 22, Raising the blast time to 0.007 seconds has the most impact on D=0.5 in scenarios two and three, where the distance is less than 3 meters. Here, the wall has %81 of concrete with less than %50 of damages with modified Jonson-Holmquist criterion, while with 0.005 seconds of blast time, we had almost %90 of concrete with the same damages. The same result can be seen for scenario three. Also, the deleted elements with %100 damages have been raised in three scenarios. Fig. 25 shows the result for 0.01 blasting time.

As shown in Fig. 23, By increasing the effective blast time and reaching 0.01 seconds, half-damage in scenarios 1 and 2 will increase significantly in far distances. Meanwhile, the complete damage elements in three scenarios have been raised too, where we face almost %11 of the deleted zone in the nearest distance of scenario one. Like shorter times, scenario one has more half-damages in all distances, and scenario two has the most elements with D=1 in shorter distances.

13. Conclusions

If they were as high as we needed, cantilever Retaining walls could make a sound barrier, while generally, they are aesthetically pleasing. Hence, whenever an explosion load is embedded in the soil, these barrier walls can significantly reduce the pressure caused by the explosion, so ultimate damage in structures and the vicinity will decrease (Agency 2003).

The blast simulation results extensively relate to the soil and structure constitutive models and characteristics. This fact states the importance of specific soil properties and utilization of proper models when assessing the behavior of vicinity structures such as concretes in retaining walls subjected to surface air of buried explosions.

Numerical simulation of TNT charge blasts in different positions has been challenging for over two decades. The current research uses the CEL method to simulate the detonation of 500 kg TNT and its effects on the cantilever retaining wall. The air, soil, and explosive load are fluid phases; therefore, they were modeled with an Euler solver, whereas a Lagrange processor is suitable for solid-phase and adopted for the concrete retaining wall. In addition, the JWL equation, the second version of the Johnson-Holmquist Equation, and Mohr-Coulomb constitutive law models are used to determine TNT's behavior, wall's concrete, and soil, respectively.

The damage rate and shape of deformations observed from the current paper match the experimental test. This fact reveals that the current code can effectively predict the dynamic behavior of cantilever-retaining walls under explosion loads. The damage rate caused by the soil mass that contacts the cantilever-reinforced wall was extensively greater than that caused by the free-air or surface contact explosion with the same explosive charge. The same result for underwater explosions has been reported by (Zhao *et al*. 2018).

The current outcomes obtained from the simulation of the retaining wall are perfect matches with the field test results reported by the US Army Corps of Engineers (Defense 2008). As expected, the maximum displacement at the center of the cantilever wall is greatly affected by the stand-off distance, which was also reported by (Lin *et al*. 2014)**.** Some conclusions can be drawn as follows:

• The current numerical simulations match the famous experimental tests, which indicate that the fully-coupled Euler–Lagrange Interaction method can deal with extensive large deformation in soil and walls the model faces in explosions.

• The values obtained for the peak pressure and blast wave arrival time in scenario two, where the charge embedded in the soil mass are very close to those reported by (Ambrosini and Luccioni 2020).

• The peak pressure in TNT explosion, the arrival time of the force, and the positive phase time are close to those reported by Lu *et al*. (2005). In that paper, A 2D simulation utilizing a combination of SPH and FEM simulation was used.

• Modified Johnson Holmquist's constitutive law model can simulate compressive damage elements and effectively predict the volumetric strains in concrete elements.

• The stress-loading rate has a massive effect on the compressive damages. The complete damage elements are also high whenever the loading rate is very high, especially at low distances. When the loading rate is relatively low, half-damage elements are raised, signifying compared to entirely damaged ones, especially far distances.

• In the air contact explosion used in scenario one, severe blast loads in distances between 1 meter to three meters lead to the perforation and concrete failure in the wall; the same event occurs in embedded TNT in the
same distance

• An obvious wall deformation was observed in the toe of the wall in the air blast of scenario one and the middle of the wall in scenario two.

• Free-air blast has the highest half-damage in all distances

• Soil-embedded blasts have been affected by distance more than free-air blasts. Soil-embedded blasts have more completely damaged elements at a low distance, while they have almost zero elements with half-damages at a distance of more than 1 meter. The same result had been reported by (Yang *et al*. 2019)

• Blast at the soil's surface beside the wall has the lowest damage, while the bending moment caused by deformation should be considered.

Overall, by considering the correlation of experimental test and numerical results in the current paper, it can be said that the proposed finite element procedure, which used the fully-coupled Euler–Lagrange Interaction method along with the modified Johnson-Holmquist method, can perfectly model the concrete damage rate while applying the dynamic loads. So, the researchers can predict the failure modes, especially in cantilever-reinforced concrete walls.

References

Abedini, M., Mutalib, A.A., Mehrmashhadi, J., Raman, S.N., Alipour, R., Momeni, T. and Mussa, M.H. (2019), *Large deflection behavior effect in reinforced concrete columns exposed to extreme dynamic loads*, https://doi.org/10.1007/s11709-020-0604-9.

Acosta, P.F. (2011), "Overview of UFC 3-340-02 structures to resist the effects of accidental explosions", *Proceedings of the Structures Congress 2011*, 1454-1469. https://doi.org/10.1061/41171(401)127.

Agency, D. of H.S.F.E.M. (2003), *Reference Manual To Mitigate Potential Terrorist Attacks Against Buildings*. Government Printing Office. https://www.dhs.gov/xlibrary/assets/st/st-bips-06.pdf.

Akram, M.R. and Yesilyurt, A. (2023), "Experimental analysis of blast loading effects on security check-post", *Struct. Eng. Mech.*, **87**(3), 273-282. https://doi.org/10.12989/sem.2023.87.3.273.

Ambrosini, D. and Luccioni, B. (2020), "Effects of underground explosions on soil and structures", *Underground Space (China)*, **5**(4), 324-338. https://doi.org/10.1016/j.undsp.2019.09.002.

Baker, W.E., Westine, P.S. and Dodge, F.T. (1973), *Similarity Methods in Engineering Dynamics, Rochelle*. NJ: Spartan Books, Hayden Book Company, Inc. https://www.elsevier.com/books/similarity-methods-in-engineering-dynamics/westine/978-0-444-88156-4

Brode, H.L. (1955), "Numerical solutions of spherical blast waves", *J. Appl. Phys.*, **26**(6), 766-775. https://doi.org/10.1063/1.1722085.

Bulson, P.S. (1997), *Explosive loading of engineering structures*, CRC Press. https://doi.org/10.4324/9780203473863.

Cheeseman, B.A., Wolf, S., Yen, C.F. andSkaggs, R. (2006), "Blast simulation of explosives buried in saturated sand", *Fragblast*, **10**(1-2), 1-8. https://doi.org/10.1080/13855140500432045.

Choi, S., Wang, J., Munfakh, G. and Dwyre, E. (2006), "3D nonlinear blast model analysis for underground structures", *Proceedings of the GeoCongress 2006: Geotechnical Engineering in the Information Technology Age* 1-6. https://doi.org/10.1061/40803(187)206.

Dadkhah, H. and Mohebbi, M. (2021), "A multi - hazard - based design approach for LRB isolation system against explosion and earthquake", *Earthq. Struct.*, **21**(1), 95-111. https://doi.org/10.12989/eas.2021.21.1.095.

De, A. (2012), "Computers and Geotechnics Numerical simulation of surface explosions over dry, cohesionless soil", *Comput. Geotech.*, **43**, 72-79. https://doi.org/10.1016/j.compgeo.2012.02.007.

Defense, U.S.D. of. (2008), Structures to resist the effects of accidental explosions. *UFC 3-340-02*. https://www.wbdg.org/ffc/dod/unified-facilities-criteria-ufc/ufc-3-340-02.

Hao, H., Hao, Y., Li, J. and Chen, W. (2016a), "Review of the current practices in blast-resistant analysis and design of concrete structures", *Adv. Struct. Eng.*, **19**(8), 1193-1223. https://doi.org/10.1177/1369433216656430.

Hao, H., Hao, Y., Li, J. and Chen, W. (2016b), "Review of the current practices in blast-resistant analysis and design of concrete structures", *Adv. Struct. Eng.*, **19**(8), 1193-1223. https://doi.org/10.1177/1369433216656430.

Hejazi, Y., Dias, D. and Kastner, R. (2008), "Impact of constitutive models on the numerical analysis of underground constructions", *Acta Geotechnica*, **3**(4), 251-258. https://doi.org/10.1007/s11440-008-0056-1.

Henrych, J. and Major, R. (1979), *The dynamics of explosion and its use*, **569**. https://doi.org/10.1063/1.46199.

Jeon, S., Kim, T.H. and You, K.H. (2015), "Characteristics of crater formation due to explosives blasting in rock mass", *Geomech. Eng.*, **9**(3), 329-344. https://doi.org/10.12989/gae.2015.9.3.329.

Jin, Z., Ning, J. and Xu, X. (2023), "A novel coupled Euler–Lagrange method for high resolution shock and discontinuities capturing", *Int. J. Numer. Method. Fluid.*, https://doi.org/10.1002/fld.5255.

Johnson, G.R. and Holmquist, T.J. (1992), "A computational constitutive model for brittle materials subjected to large strains, high strain rates and high pressures", *Shock Wave and High-Strain-Rate Phenomena in Materials*, 1075-1081.

https://doi.org/10.1063/1.46199.

Khodaparast, M., Hosseini, S.H. and Moghtadaei, H. (2023), "Determination of blast impact range and safe distance for a reinforced concrete pile under blast loading", *Int. J. Eng.*, **36**(2), 384-397. https://doi.org/10.5829/IJE.2023.36.02B.17.

Kim, D. and Park, K. (2019), "Study on the characteristics of grout material using ground granulated blast furnace slag and carbon fiber", *Geomech. Eng.*, **19**(4), 361-368. https://doi.org/10.12989/gae.2019.19.4.361.

Kinney, G.F. and Graham, K.J. (2013), *Explosive shocks in air*. Springer Science & Business Media. https://doi.org/10.1121/1.394030

Koneshwaran, S., Thambiratnam, D.P. and Gallage, C. (2015), "Blast response of segmented bored tunnel using coupled SPH–FE method", *Structures*, **2**, 58–71. https://doi.org/DOI:10.2749/101686615X14355644771054

Kucewicz, M., Baranowski, P. and Małachowski, J. (2020), "Determination and validation of Karagozian-Case Concrete constitutive model parameters for numerical modeling of dolomite rock", *Int. J. Rock Mech. Min. Sci.*, **129**, 104302. https://doi.org/10.1016/j.ijrmms.2020.104302.

Kucewicz, M., Baranowski, P. and Małachowski, J. (2021), "Dolomite fracture modeling using the Johnson-Holmquist concrete material model: Parameter determination and validation", *J. Rock Mech. Geotech. Eng.*, **13**(2), 335-350. https://doi.org/10.1016/j.jrmge.2020.09.007.

Li, X.L. (2020), *Parametric Study on Numerical Simulation of Missile Punching Test Using Concrete Damaged Plasticity (CDP) Model*, 1-2. https://doi.org/10.1016/j.ijimpeng.2020.103652.

Lin, X., Zhang, Y.X. and Hazell, P.J. (2014), "Modelling the response of reinforced concrete panels under blast loading", *Mater. Design*, **56**, 620-628. https://doi.org/10.1016/j.matdes.2013.11.069.

Liu, F., Silva, J., Yang, S., Lv, H. and Zhang, J. (2019), "Influence of explosives distribution on coal fragmentation in top-coal caving mining", *Geomech. Eng.*, **18**(2), 111-119. https://doi.org/10.12989/gae.2019.18.2.111.

Luccioni, B., Ambrosini, D., Nurick, G. and Snyman, I. (2009), "Craters produced by underground explosions", *Comput. Struct.*, **87**(21-22), 1366-1373. https://doi.org/10.1016/j.compstruc.2009.06.002.

Ma, G.W.Ã. and An, X.M. (2008), "Numerical simulation of blasting-induced rock fractures", **45**, 966-975. https://doi.org/10.1016/j.ijrmms.2007.12.002.

Mahmoud, S. (2019), "Blast-load-induced interaction between adjacent multi-story buildings", *Earthq. Struct.*, **17**(1), 17-29. https://doi.org/10.12989/eas.2019.17.1.017.

Manual, A.U. (2020), Abaqus user manual, *Abacus*. http://130.149.89.49:2080/v6.11/pdf_books/CAE.pdf.

Murthy, A., Palani, G.S. and Iyer, N.R. (2010), "Impact analysis of concrete structural components", *Defence Sci. J.*, **60**(3). https://doi.org/10.14429/dsj.60.358.

Osinov, V.A., Chrisopoulos, S. and Triantafyllidis, T. (2019), "Numerical analysis of the tunnel-soil interaction caused by an explosion in the tunnel", *Soil Dyn. Earthq. Eng.*, **122**, 318-326. https://doi.org/10.1016/j.soildyn.2018.09.010.

Oucif, C. and Muhammad, L. (2018), "Science direct numerical modeling of high velocity impact applied to reinforced concrete panel", *Undergr. Space*, https://doi.org/10.1016/j.undsp.2018.04.007.

Park, G.K., Kwak, H.G. and Filippou, F.C. (2021), "Hysteretic moment-curvature relations for the analysis of RC flexural members subjected to blast loading", *Comput. Concrete*, **27**(6), 537-548. https://doi.org/10.12989/cac.2021.27.6.537.

Rahgooy, K., Bahmanpour, A., Derakhshandi, M. and Bagherzadeh, A. (2022), "Distribution of elastoplastic modulus of subgrade reaction for analysis of raft foundations", **28(1)**, 89-105. https://doi.org/10.12989/gae.2022.28.1.089

Rashiddel, A., Kharghani, M., Dias, D. and Hajihassani, M. (2020), "Computers and Geotechnics Numerical study of the segmental tunnel lining behavior under a surface explosion – Impact of the longitudinal joints shape", *Comput. Geotech.*, **128**, 103822. https://doi.org/10.1016/j.compgeo.2020.103822.

Sagong, M., Choi, I.Y., Lee, J.S. and Cho, C. (2020), "Shear strength behaviors of grouts under the blasting induced vibrations", *Geomech. Eng.*, **21**(2), 207-213. https://doi.org/10.12989/gae.2020.21.3.289.

Schwer, L.E. and Day, J. (1991), "Computational techniques for penetration of concrete and steel targets by oblique impact of deformable projectiles", *Nuclear Eng. Design*, **125**(2), 215-238. https://doi.org/10.1016/0029-5493(91)90079-w.

Shadabfar, M., Huang, H., Wang, Y. and Wu, C. (2020), "Monte carlo analysis of the induced cracked zone by single-hole rock explosion", *Geomech. Eng.*, **21**(3), 289-300. https://doi.org/10.12989/gae.2020.21.3.289.

Station, U.S.A.E.W.E. (1986), TM5-855-1 Fundamentals of protective design for conventional weapons, *US Army, Navy and Air Force*, *US Government Printing Office*, *Washington DC*. https://catalogue.nla.gov.au/Record/4066161.

Sun, Q. and Liu, C. (2022), "Near-explosion protection method of pi-section reinforced concrete beam", *Geomech. Eng.*, **28**(3), 209-224. https://doi.org/10.12989/gae.2022.28.3.209.

Swinton, R.J. and Bergeron, D.M. (2004), *Evaluation of a silent killer, the PMN anti-personnel blast mine*, https://www.semanticscholar.org/paper/Evaluation-of-a-Silent-Killer%2C-the-PMN-Blast-Mine-Swinton-Bergeron/1ec5f180a8fbda7628cc5d110dddd57b254315bb

Tai, Y.S. and Tang, C.C. (2006), "Numerical simulation: The dynamic behavior of reinforced concrete plates under normal impact", *Theor. Appl. Fract. Mech.*, **45**(2), 117-127. https://doi.org/10.1016/j.tafmec.2006.02.007.

Tash, F.Y. and Neya, B.N. (2020), "An analytical solution for bending of transversely isotropic thick rectangular plates with variable thickness", *Appl. Math. Model.*, **77**, 1582-1602. https://doi.org/10.1243/03093247JSA666.

Tuğrul, A. and Sevim, B. (2017), "Numerically and empirically determination of blasting response of a RC retaining wall under TNT explosive", *Adv. Concrete Constr.*, **5**(5), 493-512. https://doi.org/10.12989/acc.2017.5.5.493.

Uyar, G.G. and Aksoy, C.O. (2019), "Comparative review and interpretation of the conventional and new methods in blast vibration analyses", *Geomech. Eng.*, **18**(5), 545-554. https://doi.org/10.12989/gae.2019.18.5.545.

Wang, J., Liu, F. and Zhang, J. (2019), "Investigation on the propagation mechanism of explosion stress wave in underground mining", *Geomech. Eng.*, **17**(3), 295-305. https://doi.org/10.12989/gae.2019.17.3.295.

Wu, C. and Hao, H. (2005), "Modeling of simultaneous ground shock and airblast pressure on nearby structures from surface explosions", *Int. J. Impact Eng.*, **31**(6), 699-717. https://doi.org/10.1016/j.ijimpeng.2004.03.002.

Yang, G., Wang, G., Lu, W., Wu, L., Yan, P. and Chen, M. (2019), "Experimental and numerical study of damage characteristics of RC slabs subjected to air and underwater contact explosions", *Mar. Struct.*, **66**, 242-257. https://doi.org/10.1016/j.marstruc.2019.04.009.

Zhao, C.F., Chen, J.Y., Wang, Y. and Lu, S.J. (2012), *Damage mechanism and response of reinforced concrete containment structure under internal blast loading*, **61**, 12-20. https://doi.org/10.1016/j.tafmec.2012.08.002.

Zhao, X., Wang, G., Lu, W., Yan, P., Chen, M. and Zhou, C. (2018). "Damage features of RC slabs subjected to air and underwater contact explosions", *Ocean Eng.*, **147**, 531-545.

https://doi.org/10.1016/j.oceaneng.2017.11.007.

CC